Optics Letters

Visible supercontinuum generation in a graded index multimode fiber pumped at 1064 nm

G. Lopez-Galmiche,[1,2,*] Z. Sanjabi Eznaveh,[1] M. A. Eftekhar,[1] J. Antonio Lopez,[1] L. G. Wright,[3] F. Wise,[3] D. Christodoulides,[1] and R. Amezcua Correa[1]

[1]CREOL, The College of Optics and Photonics, University of Central Florida, Orlando, Florida 32816, USA
[2]Instituto Nacional de Astrofísica Óptica y Electrónica (INAOE), Apartado Postal 51 y 216, Tonantzintla, Puebla 7200, Mexico
[3]School of Applied and Engineering Physics, Cornell University, Ithaca, New York 148853, USA
*Corresponding author: gisela.lopezgalmiche@ucf.edu

Received 25 March 2016; revised 26 April 2016; accepted 3 May 2016; posted 4 May 2016 (Doc. ID 261946); published 25 May 2016

We observe efficient supercontinuum generation that extends into the visible spectral range by pumping a low differential mode group delay graded index multimode fiber in the normal dispersion regime. For a 28.5 m long fiber, the generated spectrum spans more than two octaves, starting from below 450 nm and extending beyond 2400 nm. The main nonlinear mechanisms contributing to the visible spectrum generation are attributed to multipath four-wave mixing processes and periodic spatio-temporal breathing dynamics. Moreover, by exploiting the highly multimodal nature of this system, we demonstrate versatile generation of visible spectral peaks in shorter fiber spans by altering the launching conditions. A nonlinearly induced mode cleanup was also observed at the pump wavelength. Our results could pave the way for high brightness, high power, and compact, multi-octave continuum sources.

OCIS codes: (190.4370) Nonlinear optics, fibers; (190.4380) Nonlinear optics, four-wave mixing; (190.5650) Raman effect; (190.4410) Nonlinear optics, parametric processes.

http://dx.doi.org/10.1364/OL.41.002553

Supercontinuum generation today is finding extensive applications in biomedical imaging, optical metrology, spectroscopy, and sensing, to mention a few [1]. In this regard, extensive investigations have been carried out to develop compact, efficient, and robust fiber-based supercontinuum sources, leading to high-performance commercial products. This field experienced rapid growth with the advent of photonic crystal fibers (PCFs) that allowed for the first time an unprecedented control of dispersion and nonlinear characteristics [2–5]. On the other hand, extending the supercontinuum into the visible spectral region has always been a subject of considerable investigation. This aspect becomes particularly challenging, especially if high power densities with uniform spectral profiles are required using stable, readily available pump sources. Possible avenues to enhance visible the supercontinuum include, for example, the use of tapered photonic crystal fibers, PCFs with tailored dispersion characteristics and two-mode fiber structures [6–9].

Thus far, most of the supercontinuum generation studies have been performed almost exclusively in single-mode or few-mode fibers [1–10]. On the other hand, recently, there has been a resurgence of interest in multimode fiber systems, both in the linear and nonlinear domain [11–14]. Additionally, in the past few years, rapid progress has been made in developing advanced graded index multimode fibers (MMFs) and few-mode fibers with precisely engineered differential mode group delays (DMGD) [15,16]—thus providing a rich platform for exploring complex multimode nonlinear dynamics.

In general, multimode fibers can handle higher power levels and enable a multitude of interactions between their many supported spatial modes that would have been otherwise impossible in single-mode settings. Intermodal Raman and four-wave mixing (FWM) frequency conversions have been studied in MMFs under various conditions [17–20]. Recently, multimoded solitons, as well as supercontinuum generation, have been successfully demonstrated in graded index optical fibers by launching ultra-short pulses in the anomalous dispersion regime (1550 nm) [13,21,22]. Interestingly, in these experiments, discrete spectral components were observed in the visible domain. These features were subsequently explained through the interplay between spatio-temporal soliton oscillations and dispersive waves that are possible in parabolic fibers [23].

Here we report visible supercontinuum generation in a low differential modal group delay multimode graded index fiber with a core diameter of 50 μm (WideCap MMF fabricated by Prysmian Group), pumped in the normal dispersion regime. The observed spectrum was found to extend from 450 to 2400 nm, resulting from a geometric parametric instability. Despite the fact that the fiber supports hundreds of transverse modes, the output intensity distributions appear to be Gaussian-like and speckle free. This beam cleanup process leads to improved beam quality factors (M^2) at the pump wavelength. The M^2 of the output intensity profiles was measured for various wavelengths, and the spectral evolution of the continuum was obtained as a function of pump power and fiber length. In addition, we found that the generated spectrum

depends on the initial excitation conditions, thus establishing new degrees of freedom for developing tunable all-fiber sources. Our experiments indicate that these processes can be utilized for generating tunable, ultrabroadband, relatively flat supercontinuum spectra with high average power densities.

Figure 1 shows a schematic of the experimental setup. The single-mode output of an amplified Q-switched micro-chip laser, delivering 95 μJ pulses at 1064 nm, with a pulse duration of 400 ps and a repetition rate of 500 Hz, was coupled into the MMF. The free space coupling efficiency was greater than 85% using a 50 mm focal length lens. The coupling was stable for several hours, even at high power levels. To keep the coupling conditions invariant with respect to the input power, a half wave plate and a polarizing beam splitter cube (PBSC) were used. The initial spatial launching conditions were adjusted using a three-axis translation stage. A large set of transverse spatial modes was excited at the fiber input by focusing the laser beam to ~27 μm. Light at the output of the MMF under test was collected by a multimode patch cord (105 μm core diameter) and analyzed using optical spectrum analyzers (OSAs) covering the spectral range from 350 to 1750 nm (ANDO AQ 6315E) and 1200 to 2400 nm (Yokogawa AQ6375). Infrared and visible cameras were employed to record the beam profiles at the output.

The fiber used in the experiments was a trench-assisted graded index MMF with a core diameter of 50 μm and refractive index contrast of $\sim 1.6 \times 10^{-2}$. Although the fiber was coiled in a 15 cm diameter reel, higher-order modes were guided with very low losses due to the fiber's trench-assisted design. A typical image of the visible spectrum, obtained in a 28.5 m long fiber for a pump peak power of ~185 kW, is displayed in Fig. 2(a) after being dispersed by a diffraction grating. This image shows a rather uniform generated spectrum, from deep red to purple, having only discrete peaks in the blue. As we will see, the main nonlinear mechanisms contributing to the visible spectrum generation arise from multipath four-wave mixing processes and periodic spatio-temporal breathing dynamics.

The generated supercontinuum spectrum in the 28.5 m long fiber under the same launching conditions, measured using two different OSAs, is presented in Fig. 2(b). One can observe that the input pulses produce a remarkable spectral broadening on both sides of the pump, extending from ~450 to more than 2400 nm. Figure 2(b) clearly demonstrates that in this low DMGD MMF, supercontinuum generation spectrally unfolds in a rather uniform fashion between 600 and 1750 nm. On the other hand, the spectrum involves a series of FWM and Raman peaks on top of this uniform supercontinuum. In the longer spans (28.5 m), the supercontinuum was found to be stable and relatively insensitive to alignment.

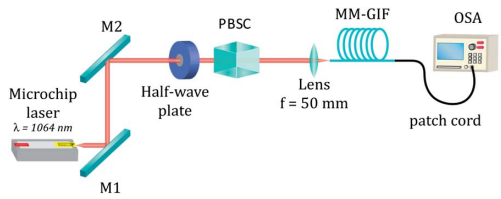

Fig. 1. Schematic of the experimental setup. Pulses from a Q-switched microchip laser at 1064 nm are coupled into a graded index MMF.

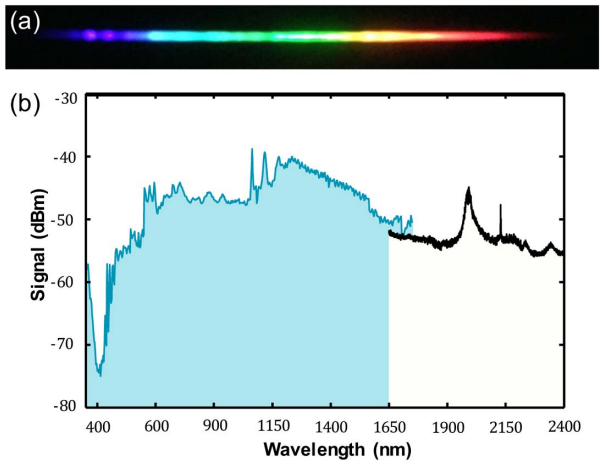

Fig. 2. Experimental supercontinuum spectra obtained in a 28.5 m long graded index MMF using 185 kW peak pump power at 1064 nm. (a) Image of the visible component of the dispersed output spectrum. (b) Spectrum recorded using two different OSAs covering the spectral range from 350 to 2400 nm.

Subsequently, we characterized the spatial mode profile of the fiber output at various wavelengths using 10 nm bandpass filters and appropriate imaging cameras; see Fig. 3. Interestingly, at high power levels, the spatial mode distributions do not exhibit a speckle structure. Instead, the mode profiles are Gaussian-like for all measured wavelengths. At the pump wavelength, a nonlinear spatial cleanup process is found to take place in this graded index MMF. Figure 4 depicts the evolution of this mechanism as a function of pump power at 1064 nm in a 1.3 m long fiber, for two initial spatial intensity distributions, Figs. 4(a)–4(c) and Figs. 4(d)–4(f), respectively. While at low power [1.5 W, Figs. 4(a) and 4(d)], the output mode profiles are considerably speckled; at the higher input powers of 35 and 50 kW, a beam cleanup is evident [Figs. 4(b)–4(d) and Fig. 4(f)]. This effect is induced by the Kerr nonlinearity and is unrelated to Raman filtering effects. We note that similar effects have been recently observed by Krupa *et al.* [24]. Remarkably, the M^2 is significantly reduced from 7.5 to 2.1 during this process in a 1.3 m long fiber, corresponding to Figs. 4(a) and 4(c), respectively. This represents a significant increase in the beam brightness. Given that Raman cleanup is not a factor at the pump wavelength, we attribute these effects to four-wave-mixing processes. In addition, the modal cleanup happens to be quite robust to intentional fiber bends and twists.

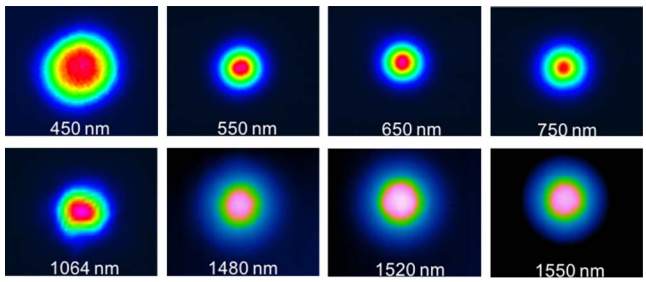

Fig. 3. Near-field beam profiles in the visible and near infrared at the output of a 28.5 m multimode optical fiber at 185 kW pump power.

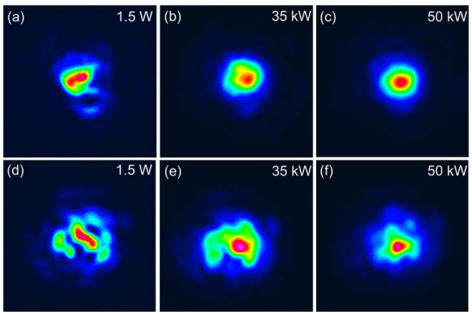

Fig. 4. Evolution of the MMF output beam profile at 1064 nm in a 1.3 m MMF, as a function of input power for two initial launching conditions (a)–(c) and (d)–(f), respectively.

This property could be potentially useful in high power delivery applications where a stable, high-brightness beam profile output is desirable.

In addition, the beam quality factor M^2 was measured in the wavelength range of 550 to 1064 nm, as shown in Fig. 5, for the 28.5 m long MMF. Our observations clearly indicate that the M^2 values tend to decrease as the wavelength increases. To some extent, this is due to the fact the number of supported modes also decreases at longer wavelengths. The large M^2 values observed in Fig. 5 are attributed to the presence of a broad multimoded pedestal (see also Fig. 3) that accompanies the Gaussian-like intensity profile.

To better understand the evolution of the continuum as a function of pump power and fiber length, we have performed a series of measurements for different power levels and fiber spans. Figure 6 shows typical spectra for varying input powers, at 6 m [Figs. 6(a)–6(d)] and 11 m [Figs. 6(e)–6(h)], using a 350–1750 nm OSA. For these measurements, the fiber was excited at the center with a spot size diameter of ~27 μm. At 28 kW input pump power, Raman generation and some self-phase modulation takes place [Fig. 6(a)]. At 85 kW, additional discrete frequency peaks appear in the spectrum [Fig. 6(b)]. The feature at ~0.8 PHz is due to third-harmonic generation from the pump itself and its first Stokes line. To explain the frequency generation between 0.3 and 0.7 PHz shown in Fig. 6(b), we use the theoretical model developed by Longhi [25]. In this approach, the spatio-temporal modulation instability occurring in a parabolic optical fiber (geometric parametric instability or GPI) is analyzed in terms of a Floquet–Bloch theory, in both the normal and anomalous dispersion regimes. What is intriguing in this case is that modulation instability can

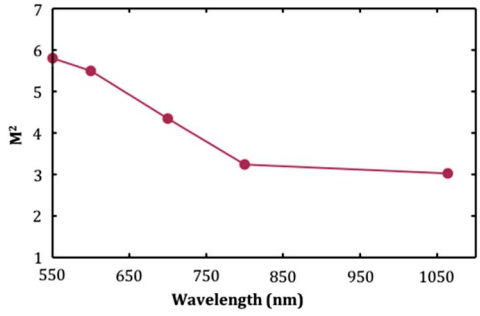

Fig. 5. Measured beam quality factor as a function of the wavelength at the output of the MMF.

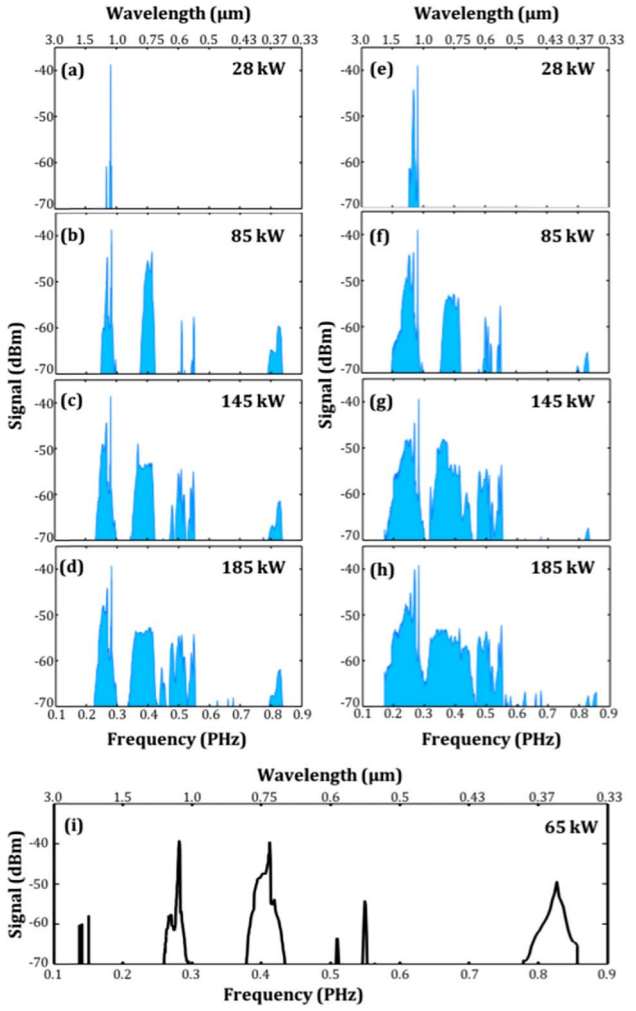

Fig. 6. Supercontinuum evolution as a function of pump power and fiber length. (a)–(d) for a MMF length of 6 m, and (e)–(h) for a MMF length of 11 m, for input powers of 28 kW, 85 kW, 145 kW, and 185 kW. (i) Spectral lines in the NIR ~1960 nm produced by the spatio-temporal instability that is also responsible for shaping up the supercontinuum generation in the visible for a fiber length of 1.3 m and pump power of 65 kW.

always occur, even in the normal dispersive region, because of periodic focusing events that are known to take place in graded index fibers [22]. Under these conditions, the frequency separation between the modulation instability sidebands is given by [25,26] $\omega_m^2 = (2m\delta/k_0'') - (2n_2 I\omega_0/ck_0'')$, where δ stands for the spacing between the propagation constants of consecutive modes $\delta = a^{-1}\sqrt{2\Delta}$, with $\Delta = \frac{n_{\text{core}} - n_{\text{clad}}}{n_{\text{core}}}$, and a being the core radius. In the above equation, m is an integer $m = 1, 2, 3, \ldots$, n_2 is the nonlinear Kerr coefficient, and ω_0 and I represent the angular frequency and intensity of the pump, respectively. In addition, at 1064 nm, the fiber dispersion coefficient is $k_0'' = 1.75 \times 10^{-26}$ m^{-1} s^2. In obtaining the latter equation, we assumed that only radially symmetric modes (LP_{0m}) are involved, i.e., the fiber is symmetrically excited at the center. Clearly, if the input spot size does not match that of the Gaussian fundamental mode LP_{01}, a periodic compression/expansion will initially occur in the transverse

plane and, hence, in time. It is this periodic breathing that leads to the generation of the frequency sidebands ω_m. In our experiment, $a = 25$ μm, $\Delta \approx 10^{-2}$, and the maximum peak power used was 185 kW over an initial spot size of 27 μm in diameter at the fiber input face. For these parameters, the spatio-temporal oscillation period is $\pi a(2\Delta)^{-1/2} \approx 550$ μm, and the nonlinear term in the ω_m expression is negligible. As a result, $\omega_m \approx (2m\delta/k_0'')^{1/2}$. For the first sidebands $m = 1$, and $f_1 = 128$ THz. Therefore, two sidebands first emerge symmetrically around the pump, at NIR ~1.96 μm, (153 THz) and in the visible at ~0.73 μm, (410 THz) that is prominently shown in our spectrum of Fig. 6(b). Similarly, the other discrete peaks in the visible [Fig. 6(b)] result from higher-order sidebands ω_m and their respective FWM combinations. Some of them clearly appear at higher pump powers, as depicted in Figs. 6(c) and 6(d). Subsequently, these spectral peaks broaden via self-phase-modulation, FWM and Raman, thus eventually generating supercontinuum for longer propagation distances [Figs. 6(e)–6(h)]. A further increase in the fiber length leads to the uniform supercontinuum generation depicted in Fig. 2(b). To verify the existence of the NIR ~1960 nm line, arising from the aforementioned spatio-temporal breathing instability, the spectrum was separately measured in the 1650–2400 nm range using a Yokogawa OSA for a fiber length of 1.3 m and 65 kW input peak power. The presence of the ~1960 nm spectral peak that is also to a great extent responsible for shaping the visible generation is clearly evident in this figure.

In summary, we demonstrated ultra-broad supercontinuum generation using a graded index multimode optical fiber pumped in the normal dispersion regime at 1064 nm. We showed that the visible spectrum generation was triggered by modulation instabilities due to periodic focusing events taking place in the low DMGD parabolic MMF. While the generated spectrum is comparable to that previously observed in endlessly single-mode PCFs [8], the use of large core MMFs offers unprecedented opportunities for power-scalable nonlinear fiber sources. In principle, the large MMF core areas could allow orders of magnitude higher spectral densities to be generated, in comparison to single-mode structures. A nonlinearly induced mode cleanup was also demonstrated at the pump wavelength. Finally, of interest would be to further study the effect of the fiber refractive index profile, pump modal content, wavelength, and pulse duration on the evolution of supercontinuum generation in such heavily multimoded environments.

Funding. Office of Naval Research (ONR) (MURI N00014-13-1-0649); HEL-JTO; Army Research Office (ARO) (W911NF-12-1-0450); CONACyT.

Acknowledgment. The authors thank the Prysmian Group for providing the WideCap low-DMGD MMF. Gisela Lopez-Galmiche was supported by a student grant by CONACyT, Mexico.

REFERENCES

1. J. M. Dudley, G. Genty, and S. Coen, Rev. Mod. Phys. **78**, 1135 (2006).
2. T. A. Birks, J. C. Knight, and P. St.J. Russell, Opt. Lett. **22**, 961 (1997).
3. J. K. Ranka, R. S. Windeler, and A. J. Stentz, Opt. Lett. **25**, 25 (2000).
4. W. J. Wadsworth, N. Joly, J. C. Knight, T. A. Birks, F. Biancalana, and P. St.J. Russell, Opt. Express **12**, 299 (2004).
5. W. J. Wadsworth, A. Ortigosa-Blanch, J. C. Knight, T. A. Birks, T. P. M. Man, and P. St.J. Russell, J. Opt. Soc. Am. B **19**, 2148 (2002).
6. C. Xiong, A. Witkowska, S. G. Leon-Saval, T. A. Birks, and W. J. Wadsworth, Opt. Express **14**, 6188 (2006).
7. A. Kudlinski, A. K. George, J. C. Knight, J. C. Travers, A. B. Rulkov, S. V. Popov, and J. R. Taylor, Opt. Express **14**, 5715 (2006).
8. J. M. Stone and J. C. Knight, Opt. Express **16**, 2670 (2008).
9. C. Lesvigne, V. Couderc, A. Tonello, P. Leproux, A. Barthélémy, S. Lacroix, F. Druon, P. Blandin, M. Hanna, and P. Georges, Opt. Lett. **32**, 2173 (2007).
10. A. Mussot, T. Sylvestre, L. Provino, and H. Maillotte, Opt. Lett. **28**, 1820 (2003).
11. D. J. Richardson, J. M. Fini, and L. E. Nelson, Nat. Photonics **7**, 354 (2013).
12. F. Poletti and P. Horak, Opt. Express **17**, 6134 (2009).
13. L. G. Wright, D. N. Christodoulides, and F. W. Wise, Nat. Photonics **9**, 306 (2015).
14. I. Kubat and O. Bang, Opt. Express **24**, 2513 (2016).
15. P. Sillard, M. Bigot-Astruc, and D. Molin, J. Lightwave Technol. **32**, 2824 (2014).
16. P. Sillard, D. Molin, M. Bigot-Astruc, K. de Jongh, F. Achten, A. M. Velazquez-Benitez, R. Amezcua Correa, and C. M. Okonkwo, J. Lightwave Technol. **34**, 425 (2016).
17. R. H. Stolen, J. E. Bjorkholm, and A. Ashkin, Appl. Phys. Lett. **24**, 308 (1974).
18. H. Pourbeyram, G. P. Agrawal, and A. Mafi, Appl. Phys. Lett. **102**, 201107 (2013).
19. E. Nazemosadat, H. Pourbeyram, and A. Mafi, J. Opt. Soc. Am. B **33**, 144 (2016).
20. J. Demas, P. Steinvurzel, B. Tai, L. Rishøj, Y. Chen, and S. Ramachandran, Optica **2**, 14 (2015).
21. W. H. Renninger and F. W. Wise, Nat. Commun. **4**, 1719 (2013).
22. L. G. Wright, W. H. Renninger, D. N. Christodoulides, and F. W. Wise, Opt. Express **23**, 3492 (2015).
23. L. G. Wright, S. Wabnitz, D. N. Christodoulides, and F. W. Wise, Phys. Rev. Lett. **115**, 223902 (2015).
24. K. Krupa, A. Tonello, B. M. Shalaby, M. Fabert, A. Barthélémy, G. Millot, S. Wabnitz, and V. Couderc, "Spatial beam self-cleaning in multimode fiber," arXiv:1603.02972 (2016).
25. S. Longhi, Opt. Lett. **28**, 2363 (2003).
26. K. Krupa, A. Tonello, A. Barthélémy, V. Couderc, B. Mohamed Shalaby, A. Bendahmane, G. Millot, and S. Wabnitz, "Observation of geometric parametric instability induced by the periodic spatial self-imaging of multimode waves," arXiv:1602.04991 (2016).